


ORIGINAL ARTICLE

Open Access



Combined Estimation of Vehicle Dynamic State and Inertial Parameter for Electric Vehicles Based on Dual Central Difference Kalman Filter Method

Xianjian Jin^{1,2*} , Junpeng Yang¹, Liwei Xu³, Chongfeng Wei⁴, Zhaoran Wang¹ and Guodong Yin³

Abstract

Distributed drive electric vehicles (DDEVs) possess great advantages in the viewpoint of fuel consumption, environment protection and traffic mobility. Whereas the effects of inertial parameter variation in DDEV control system become much more pronounced due to the drastic reduction of vehicle weights and body size, and inertial parameter has seldom been tackled and systematically estimated. This paper presents a dual central difference Kalman filter (DCDKF) where two Kalman filters run in parallel to simultaneously estimate vehicle different dynamic states and inertial parameters, such as vehicle sideslip angle, vehicle mass, vehicle yaw moment of inertia, the distance from the front axle to centre of gravity. The proposed estimation method only integrates and utilizes real-time measurements of hub torque information and other in-vehicle sensors from standard DDEVs. The four-wheel nonlinear vehicle dynamics estimation model considering payload variations, Pacejka tire model, wheel and motor dynamics model is developed, the observability of the DCDKF observer is analysed and derived via Lie derivative and differential geometry theory. To address system nonlinearities in vehicle dynamics estimation, the DCDKF and dual extended Kalman filter (DEKF) are also investigated and compared. Simulation with various maneuvers are carried out to verify the effectiveness of the proposed method using Matlab/Simulink-Carsim[®]. The results show that the proposed DCDKF method can effectively estimate vehicle dynamic states and inertial parameters despite the existence of payload variations and variable driving conditions. This research provides a boot-strapping procedure which can performs optimal estimation to estimate simultaneously vehicle system state and inertial parameter with high accuracy and real-time ability.

Keywords Distributed drive, Electric vehicle, State observation, Inertial parameter, Dual central difference Kalman filter

1 Introduction

Due to the advantages of good controllability, short drive chain, compact structure, high transmission efficiency and interior space utilization, distributed drive electric vehicles (DDEVs) represent the development direction of

new energy vehicles in the future [1–3]. With the rapid development of electronic and information technology, there are more and more effective vehicle active safety systems, such as direct yaw control system (DYC) [4–6], active front steering system (AFS) [3, 7–9], anti-lock braking systems (ABS) [10, 11], active suspension system (ASS) [7, 12], electric power steering system (EPS) [13]. The accurate and real-time knowledge of vehicle dynamic state and parameters are keys and necessary conditions to realize the active safety control for DDEVs. However,

*Correspondence:

Xianjian Jin
xianjianjin@shu.edu.cn

Full list of author information is available at the end of the article



© The Author(s) 2023. **Open Access** This article is licensed under a Creative Commons Attribution 4.0 International License, which permits use, sharing, adaptation, distribution and reproduction in any medium or format, as long as you give appropriate credit to the original author(s) and the source, provide a link to the Creative Commons licence, and indicate if changes were made. The images or other third party material in this article are included in the article's Creative Commons licence, unless indicated otherwise in a credit line to the material. If material is not included in the article's Creative Commons licence and your intended use is not permitted by statutory regulation or exceeds the permitted use, you will need to obtain permission directly from the copyright holder. To view a copy of this licence, visit <http://creativecommons.org/licenses/by/4.0/>.

these fundamental vehicle dynamic state and parameters such as vehicle sideslip angle, vehicle mass, yaw moment of inertia are difficult to measure directly from standard vehicles owing to both economic and technical reasons, so these states and parameters need to be estimated or observed [14–16].

Vehicle state estimation based on vehicle dynamics model has long been an active research topic [17–20]. Typical types of observation techniques include Kalman filter (KF) [17, 18], extended Kalman filter (EKF) [19, 20], Luenberger observer [21], sliding mode observer (SMO) [22], and other non-linear observers [23, 24]. Although a lot of research achievements have been made in vehicle state observation, the research on vehicle inertial parameters observation is relatively less. In practice, the control performance of vehicle dynamics active safety system is sensitive for vehicle inertial parameters variations such as the number of passengers and the freight loading weights, the variations of vehicle inertial parameter will also affect the accuracy of state observation, so it is necessary to simultaneously estimate vehicle dynamic states combined with inertial parameters [25–27]. For instance, in Refs. [26, 27], real-time centre of gravity (CG) position estimators based on a combined adaptive Kalman filter-extended Kalman filter (AKF-EKF) approach and a novel H ∞ -extended Kalman filter (H ∞ -EKF) joint estimation method are designed respectively. In Ref. [28], the parameters of articulated heavy vehicle including the height of sprung mass CG and roll moment of inertia were estimated based on dual extended Kalman filter (DEKF). In Refs. [29, 30], an unscented Kalman filter (UKF) algorithm was introduced for state parameter estimation by extending the vehicle mass, the height of CG, and yaw moment of inertia into the vehicle state vector, which are significantly influenced by the driving state. The work [31] investigated the estimation of yaw rate, roll velocity, yaw moment and the distance from the mass center to the second axle for 8x8 distributed electric vehicles.

Compared with observers-based vehicle estimation, Kalman filters have the advantages of simple operation, good stability, real-time fast update and process for the collected data and information when dealing with the vehicle state and parameters estimation [25–27]. More recently, central difference Kalman filter (CDKF), which is based on weighted statistical linear regression and sterling interpolation formula, can adapt strongly nonlinear vehicle dynamics estimation systems [24, 32]. Thereby, the main work of this paper is to propose a dual central difference Kalman filter (DCDKF) that to simultaneously estimate vehicle state and inertial parameters of DDEVs. A nonlinear vehicle dynamics model with the payload

variations is established. Utilizing multi-sensor data fusion from the hub torque and other measurements of a standard vehicle, a parallel CDKF observation system is designed, where the first CDKF estimates the sideslip angle, yaw rate, and longitudinal velocity, and the second CDKF estimates the vehicle mass, the distance from the front axle to CG and yaw moment of inertia.

The rest content of this article is organized as follows. In Section 2, vehicle dynamics including non-linear vehicle dynamics model, tire model, wheel and motor dynamics model, is presented. Section 3 gives the design of DCDKF for vehicle states and parameters estimation. In Section 4, simulation results are given. Finally, conclusions are summarized in Section 5.

2 Vehicle System Dynamics Model

2.1 Nonlinear Vehicle Dynamics Model

The establishment of multi-degree-of-freedom nonlinear vehicle dynamics model is the basis of solving the vehicle motion state. Meanwhile, the vehicle model is a very complex system, but in order to improve the real-time performance of the vehicle state and parameters estimation, it is necessary to simplify the complex vehicle dynamic model and make some assumptions. To reflect the fundamental dynamic characteristics of the study, the 3-DOF dynamics model including longitudinal, lateral, and yaw motions of DDEVs considering uncertain load parameters shown in Figure 1 is established. Some assumptions for the non-linear vehicle model are as follows. The influence of steering transmission mechanism on the angle of two front wheels is neglected. Assuming that the vehicle moves in plane, the roll and pitch motions and their coupling, the jump between the chassis and body are ignored. The sprung mass and the unsprung mass are unified as the vehicle mass in the vehicle inertia parameters. The influence of wheel camber angle and aligning torque on vehicle dynamic performance is also ignored. In what follows, the dynamics equations by applying D’Alembert’s principle [2, 4] can be expressed as:

Longitudinal motion

$$M_t(\dot{v}_x - v_y r_z) = \sum F_{tx}^{ij} - F_f - F_a, \tag{1}$$

$$a_x = \frac{1}{M_t} \left(\sum F_{tx}^{ij} - F_f - F_a \right), \tag{2}$$

$$F_a = \frac{\rho_a C_a S v_x^2}{2}, F_f = \mu M_t g, \tag{3}$$

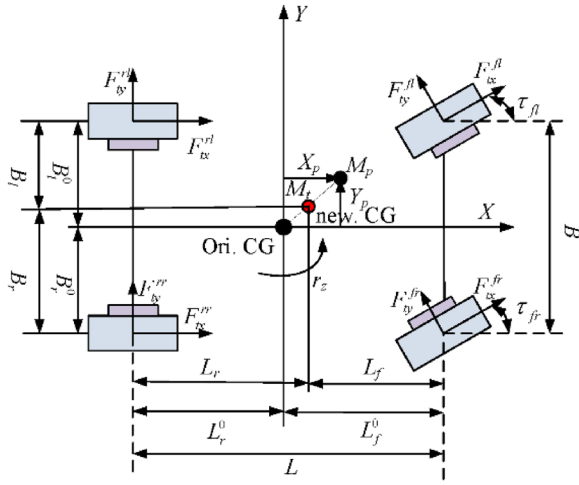


Figure 1 3-DOF dynamics model considering uncertain load parameters

$$\sum F_{tx}^{ij} = F_{tx}^{fl} \cos \tau_{fl} + F_{tx}^{fr} \cos \tau_{fr} - F_{ty}^{fl} \sin \tau_{fl} - F_{ty}^{fr} \sin \tau_{fr} + F_{tx}^{rr} + F_{tx}^{rl} \quad (4)$$

Lateral motion

$$M_t(\dot{v}_y + v_x r_z) = \sum F_{ty}^{ij} \quad (5)$$

$$a_y = \frac{1}{M_t} \sum F_{ty}^{ij} \quad (6)$$

$$\sum F_{ty}^{ij} = F_{ty}^{fl} \cos \tau_{fl} + F_{tx}^{fl} \sin \tau_{fl} + F_{ty}^{fr} \cos \tau_{fr} + F_{tx}^{fr} \sin \tau_{fr} + F_{ty}^{rl} + F_{ty}^{rr} \quad (7)$$

Yaw motion

$$I_z \dot{r}_z = M_z, \quad (8)$$

$$\begin{aligned} M_z = & (F_{ty}^{fl} \sin \tau_{fl} - F_{tx}^{fl} \cos \tau_{fl}) B_l \\ & + (F_{tx}^{fr} \cos \tau_{fr} - F_{ty}^{fr} \sin \tau_{fr}) B_r \\ & - (F_{ty}^{rr} + F_{ty}^{rl}) L_r + (F_{tx}^{fl} \sin \tau_{fl} \\ & + F_{ty}^{fl} \cos \tau_{fl} + F_{tx}^{fr} \sin \tau_{fr} \\ & + F_{ty}^{fr} \cos \tau_{fr}) L_f + (F_{tx}^{rr} B_r - F_{tx}^{rl} B_l). \end{aligned} \quad (9)$$

Besides,

$$\beta = \tan^{-1}(v_y / v_x), \quad (10)$$

where M_t is the total mass of the vehicle. r_z is the yaw rate of the vehicle. v_y, v_x are the lateral and longitudinal velocities of the vehicle. F_f, F_a are the frictional and air resistance. ρ_a, C_a and S are the air density, air resistance coefficient, and frontal windward area of the vehicle, respectively. μ is the tire-road friction coefficient. F_{ty}^{ij}, F_{tx}^{ij} are the tire-road lateral and longitudinal force, and superscript i means front or rear, superscript j means left or right. τ_{fl}, τ_{fr} are the left and right steering angle about front wheels, respectively. a_y, a_x are the lateral and longitudinal acceleration. L_f, L_r stand for horizontal distance from CG to the front and rear axles of the vehicle, and B_f, B_r stand for horizontal distance from CG to the left and right wheel, respectively. M_z, I_z are the yaw moment and yaw moment of inertia, respectively. Meanwhile, β is the sideslip angle at CG.

2.2 Vehicle Payload Parameter Analysis

When an empty vehicle is loaded with passengers or cargo, its position of CG and yaw moment of inertia will change. Meanwhile, the extra loads are not loaded at the CG but at a non-CG of the vehicle according to real-world application. In addition, considering that the change of CG height under load and unload is very small, it is assumed that the CG height of the whole vehicle does not change. When M_p at position $r_p=(X_p, Y_p)$ relative to the original coordinate system is loaded, according to the lever principle, the coordinate $r_n=(X_p, Y_p)$ of the new CG in the original coordinate system is:

$$\begin{cases} X_t = X_p \times \frac{M_p}{M_t}, \\ Y_t = Y_p \times \frac{M_p}{M_t}. \end{cases} \quad (11)$$

The relevant geometry of the vehicle varies as follows:

$$\begin{cases} L_f = L_f^0 - X_t, \\ L_r = L_r^0 + X_t, \\ L = L_f + L_r, \\ B_l = B_l^0 - Y_t, \\ B_r = B_r^0 + Y_t, \\ B = B_l + B_r. \end{cases} \quad (12)$$

Meanwhile, the yaw moment of inertia after loading is deduced as follows.

The yaw moment of inertia at the original CG after loading is deduced as:

$$I_z^n = I_z^0 + M_p \|r_p\|_2^2. \quad (13)$$

By the theorem of parallel axes [24], we get the following results:

$$I_z^n = I_z + M_t \|r_n\|_2^2. \tag{14}$$

Then,

$$I_z = I_z^0 + M_p \|r_p\|_2^2 - M_t \|r_n\|_2^2. \tag{15}$$

Using the theorem of leverage [24], the position coordinates of new CG located in the initial coordinate system are calculated:

$$M_t r_n = M_p r_p + M_s \mathbf{0}. \tag{16}$$

It can be concluded from Eq. (17):

$$r_n = (M_p / M_t) r_p. \tag{17}$$

Then the yaw moment of inertia can be further expressed as:

$$\begin{aligned} I_z &= I_z^0 + M_p \left(1 - \frac{M_p}{M_s + M_p}\right) \|r_p\|_2^2 \\ &= I_z^0 + M_p \left(1 - \frac{M_p}{M_s + M_p}\right) (X_p^2 + Y_p^2). \end{aligned} \tag{18}$$

In the above equations, M_s is the total mass of the vehicle when unloaded. B_l^0, B_r^0 are the horizontal distance between left and right wheels to CG when unloaded. L_f^0, L_r^0 are the horizontal distance from the front and rear axles of the vehicle to CG when unloaded. I_z^0 is the yaw moment of inertia when unloaded.

2.3 Vehicle Tire Model

Tire, as an important part of the interaction between the moving electric vehicle and the ground, not only supports the whole vehicle, but also transfers longitudinal and lateral forces to realize the acceleration, driving, braking and steering functions of the vehicle. Tire models can be divided into experiential models and physical models. The former gives formula to predict tire characteristics by interpolating and fitting based on tire test data. And the latter is established based on the interaction mechanism and mechanical relationship between tire and road surface. Here, the semi-empirical Pacejka tire model which uses the same set of compound trigonometric function formula to express the tire lateral force and longitudinal force is selected. The model has strong uniformity and can describe all the steady-state dynamics characteristics of the tire. It can be expressed as follows [24]:

$$\begin{cases} y = D \sin(C \tan^{-1}(Bx - EBx + E \tan^{-1}(Bx))), \\ Y(x) = y(x) + S_c, \\ x = X + S_s, \end{cases} \tag{19}$$

where the output variable Y and input variable X represent the tire force F_{ty}^{ij}, F_{tx}^{ij} and tire slip rate S_t^{ij} or slip angle α_t^{ij} . D, C, B and E are the tire model parameters: peak factor, stiffness factor, curve shape factor and curve curvature factor which are determined by the tire characteristic curve. S_s, S_c refer to the curves of horizontal drift and vertical drift.

The lateral and longitudinal forces are calculated as follows:

$$F_{ty}^{ij} = D_{ij} \sin \left[C_{ij} \tan^{-1} \left\{ \begin{aligned} &B_{ij} S_t^{ij} - E_{ij} S_t^{ij} \\ &+ E_{ij} \tan^{-1} (B_{ij} \alpha_t^{ij}) \end{aligned} \right\} \right], \tag{20}$$

$$F_{tx}^{ij} = D_{ij} \sin \left[C_{ij} \tan^{-1} \left\{ \begin{aligned} &B_{ij} S_t^{ij} - E_{ij} S_t^{ij} \\ &+ E_{ij} \tan^{-1} (B_{ij} S_t^{ij}) \end{aligned} \right\} \right]. \tag{21}$$

The calculation of parameters D, C, B, E from Ref. [24] is shown in Table 1, where $a_t^1, a_t^2, b_t^1, b_t^2$ are the calculation coefficient of crest factor, $a_t^3, a_t^4, a_t^5, b_t^3, b_t^4, b_t^5$ are the calculation coefficient of BCD, and $a_t^6, a_t^7, a_t^8, b_t^6, b_t^7, b_t^8$ are the calculation coefficient of curvature factor. Also, these parameters are related to the road adhesion coefficient, it means that the robustness of this model for different roads can be guaranteed.

The vertical load of the tire includes static load and dynamic load. The static load is obtained by the whole vehicle mass, CG position and load mass and the center of mass, while the dynamic vertical load is affected by the acceleration of the vehicle body. So the vertical load can be described as:

$$F_{zt}^{fl} = \frac{M_t}{(B_l + B_r)(L_f + L_r)} (L_r g B_r - H L_r a_y - H B_r a_x), \tag{22}$$

$$F_{zy}^{fr} = \frac{M_t}{(B_l + B_r)(L_f + L_r)} (L_r g B_l + H L_r a_y - H B_l a_x), \tag{23}$$

$$F_{tz}^{rl} = \frac{M_t}{(B_l + B_r)(L_f + L_r)} (L_f g B_r - H L_f a_y + H B_r a_x), \tag{24}$$

Table 1 Calculation of related parameters of Pacejka tire model

Variables	Lateral force	Longitudinal force
x	a	s
C	1.3	1.65
D	$b_t^1 F_{tz}^2 + b_t^2 F_{tz}$	$a_t^1 F_{tz}^2 + a_t^2 F_{tz}$
E	$b_t^6 F_{tz}^2 + b_t^7 F_{tz} + b_t^8$	$a_t^6 F_{tz}^2 + a_t^7 F_{tz} + a_t^8$
BCD	$b_t^3 \sin (b_t^4 \tan^{-1} (b_t^5 F_{tz}))$	$(a_t^3 F_{tz}^2 + a_t^4 F_{tz}) e^{-a_t^5 F_{tz}}$

$$F_{tz}^{rr} = \frac{M_t}{(B_l + B_r)(L_f + L_r)} (L_f g B_l + H L_f a_y + H B_l a_x), \quad (25)$$

where H is the height of CG.

The tire slip angle can be described as:

$$\alpha_t^{fl} = \tau_{fl} - \tan^{-1} \left(\frac{v_y + r_z L_f}{v_x - r_z B_l} \right), \quad (26)$$

$$\alpha_t^{fr} = \tau_{fr} - \tan^{-1} \left(\frac{v_y + r_z L_f}{v_x + r_z B_l} \right), \quad (27)$$

$$\alpha_t^{rl} = -\tan^{-1} \left(\frac{v_y - r_z L_r}{v_x - r_z B_l} \right), \quad (28)$$

$$\alpha_t^{rr} = -\tan^{-1} \left(\frac{v_y - r_z L_r}{v_x + r_z B_l} \right). \quad (29)$$

Similarly, the longitudinal slip rate of the tire on the four wheels can be obtained by:

$$S_t^{fl} = \frac{w_t^{fl} R_e}{(v_x - B r_z) \cos \tau_{fl} + (v_y + L_f r_z) \sin \tau_{fl}} - 1, \quad (30)$$

$$S_t^{fr} = \frac{w_t^{fr} R_e}{(v_x + B r_z) \cos \tau_{fr} + (v_y + L_f r_z) \sin \tau_{fr}} - 1, \quad (31)$$

$$S_t^{rl} = \frac{w_t^{rl} R_e}{v_x - B r_z} - 1, \quad (32)$$

$$S_t^{rr} = \frac{w_t^{rr} R_e}{v_x + B r_z} - 1, \quad (33)$$

where w_t^{ij} ($ij=fl, fr, rl, rr$) is the wheel angular velocity. R_e is the effective radius of vehicle tire.

2.4 Wheel and Motor Dynamics Model

Hub motor, as the power source and important component of DDEVs, is directly installed in the four drive wheels. The motor selection should meet the driving requirements of maximum speed, acceleration performance, climbing ability, etc. Here, permanent magnet brushless DC motor is selected [3, 31], the control circuit for the motor is simplified into a resistor-inductor (RL) circuit, which consists of a resistor and an inductance element in series. The mathematical formulation of the wheel and motor model in Figure 2 can be given by:

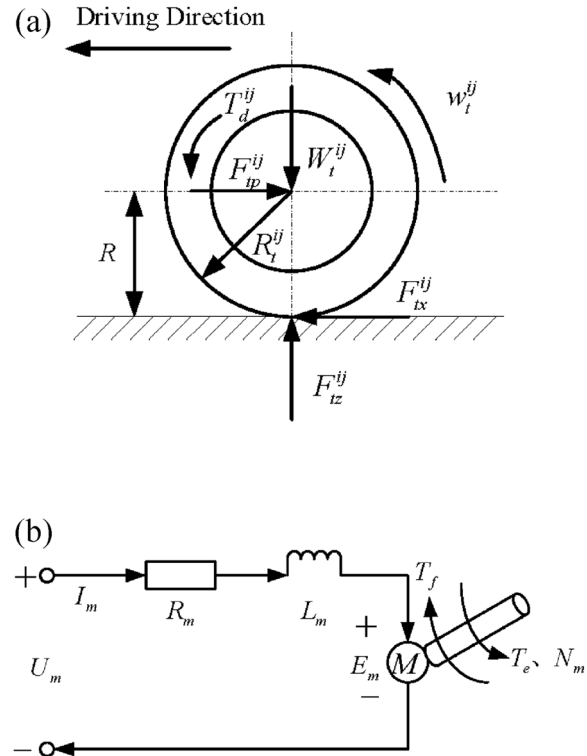


Figure 2 Wheel and motor dynamics model: (a) Wheel dynamics model, (b) Motor dynamics model

$$I_{wt}^{ij} \dot{w}_t^{ij} = T_d^{ij} - R_t^{ij} F_{xij}, \quad (34)$$

$$R_t^{ij} = R_e, \quad (35)$$

where I_{wt}^{ij} represents the equivalent moment of inertia of each wheel. T_d^{ij} represents the motor output torque, R_t^{ij} is the wheel rolling radius.

$$\begin{cases} E_m = N_m C_e, \\ \mathbf{U}_m = L_m \frac{d\mathbf{I}_m}{dt} + R_m \mathbf{I}_m + E_m, \\ T_e = C_m \mathbf{I}_m, \\ T_e - T_f = I_{wt} \frac{dN_m}{dt}, \end{cases} \quad (36)$$

where \mathbf{U}_m , E_m stand for the motor input voltage and the electromotive force of armature induction line, respectively. T_e , T_f stand for the motor load torque and the output of electromagnetic torque. N_m is the motor speed. \mathbf{I}_m , R_m , L_m stand for motor armature current, armature resistance, inductance. C_e , C_m stand for the ratio of torque to speed and the ratio of electromotive force to speed under rated excitation of motor, respectively. F_{ip}^{ij} , W_t^{ij} are the wheel resistance and gravity. R is the tire radius. The wheel model Eqs. (34), (35) and the motor

model Eq. (36) can be combined in this paper because there is no need for a transmission device to transfer the power between the wheel axle and motor.

It is worth noting that the main purpose of above vehicle system dynamics model is to design the DCDKF estimator, the simulation model built from Carsim® will be described later.

3 DCDKF Estimation Design

Note that CDKF is an KF algorithm which approximates the derivatives of nonlinear systems by polynomials with Sterling interpolation formula to avoid derivation operation, so as it can be applied to improve the effect of accurate estimation of vehicle state and inertial parameters. The DCDKF design uses two parallel CDKF to estimate vehicle state and inertial parameters of the DDEVs respectively. Also, the two observers can exchange the estimation information in real time so that the influence of estimation accuracy caused by inaccurate vehicle modeling parameters and un-modeled dynamics can be reduced. As shown in Figure 3, the proposed logic block diagram of the whole DCDKF consists of state observer and parameter observer. Note that the unique characteristics of DDEVs and the advantages of multi information sources from in sensor-wheel motor and X-by-wire systems can support the design of DCDKF system.

In order to design a combined observation system for the state and parameters of DDEVs, the following discrete system equations including the state and parameters to be estimated of the vehicle system are established:

$$\begin{cases} \mathbf{x}(t+1) = \mathbf{F}(\mathbf{x}(t), \mathbf{u}(t), \boldsymbol{\theta}(t), \mathbf{w}(t)), \\ \mathbf{y}(t+1) = \mathbf{H}(\mathbf{x}(t), \mathbf{v}(t), \boldsymbol{\theta}(t)), \end{cases} \quad (37)$$

where $F(\cdot)$ and $H(\cdot)$ represent the nonlinear function of vehicle system with regard to time. $\mathbf{u}(t)$ and $\mathbf{x}(t)$ input the

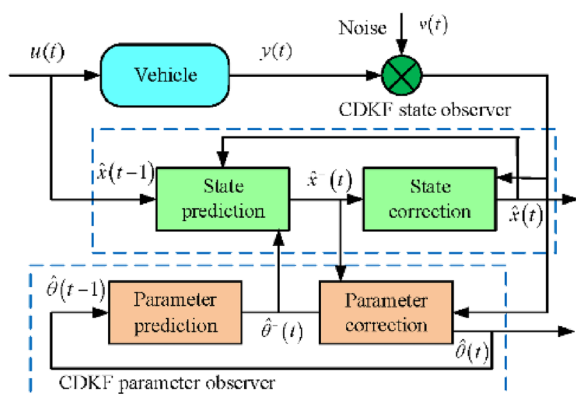


Figure 3 Logic block diagram of the whole DCDKF

vector and state vector of the vehicle system. $\mathbf{w}(t)$ and $\mathbf{v}(t)$ represent the independent zero-mean process noise and measurement noise. $\boldsymbol{\theta}(t)$ is the parameter vector.

Considering that the variation of vehicle parameters is slowly relative to states, it can be considered as a small disturbance of the system [33]. Then the parameter estimation system can be further constructed as:

$$\begin{cases} \boldsymbol{\theta}(t+1) = \boldsymbol{\theta}(t) + \mathbf{r}(t), \\ \mathbf{d}(t+1) = \mathbf{h}(\mathbf{f}(\mathbf{x}(t), \boldsymbol{\theta}(t), \mathbf{u}(t)), \mathbf{u}(t+1), \boldsymbol{\theta}(t)) + \mathbf{e}(t+1). \end{cases} \quad (38)$$

According to the system equation, the following vectors are defined.

The vehicle state vector $\mathbf{x}(t)$ includes the vehicle side-slip angle, yaw rate, longitudinal velocity:

$$\mathbf{x}(t) = [\boldsymbol{\beta}, r_z, v_x, \mathbf{a}_y]^T. \quad (39)$$

The vehicle parameter vector $\boldsymbol{\theta}(t)$ includes the vehicle mass, distance from the front axle to the CG, and yaw moment of inertia:

$$\boldsymbol{\theta}(t) = [M_t, L_f, I_z]^T. \quad (40)$$

The vehicle input vector $\mathbf{u}(t)$ includes the steering wheel angle, angular velocity of four wheels, longitudinal acceleration:

$$\mathbf{u}(t) = [\tau_f, \mathbf{w}_t^{ij}, \mathbf{a}_x]^T. \quad (41)$$

The system measurement output vector is

$$\mathbf{y}_x(t) = \mathbf{y}_\theta(t) = [r_z, \mathbf{a}_y]^T. \quad (42)$$

Next, the observability of state and parameters of the DCDKF estimation system is discussed. Note that the observability here is local. The observability of vehicle state variables can be judged based on differential geometry theory [33, 34] by using Lie derivative to solve observable matrix. While the observability of vehicle parameter vector can be judged by whether the observability co-distribution matrix is full rank or not [33, 34].

By applying the theory of differential geometry, the Lie derivatives of vehicle state system \mathbf{H} along \mathbf{F} are expressed as follows:

$$\begin{cases} L_F^0 \mathbf{H}(x) = \mathbf{H}(x), \\ L_F^l \mathbf{H}(x) = \frac{\partial (L_F^{l-1} \mathbf{H})}{\partial x} \mathbf{F}(x), l = 1, 2, 3, \dots \end{cases} \quad (43)$$

Then the observation space of the system \mathbf{A} can be expressed as:

$$V = \{H, L_F H, \dots, L_F^l H, \dots\}. \tag{44}$$

So the observability distribution of the system A is defined as follows:

$$dV(x) = \text{span}\{dV(x)|V \in V\}. \tag{45}$$

In the observation space V , $V^n = \{H, L_F H, \dots, L_F^{n-1} H\}$ is the smallest space including the measurement vector and state vector, and it is closed with respect to the Lie derivative. For $\forall x \in x^n$, if $\dim dV(x) = n$, the system is satisfied the observability conditions.

The discriminant matrix of the vehicle state observation can be written as follows:

$$dV = \begin{bmatrix} \frac{\partial(L_F^0 H)}{\partial x^T}, \frac{\partial(L_F^1 H)}{\partial x^T}, \frac{\partial(L_F^2 H)}{\partial x^T}, \frac{\partial(L_F^3 H)}{\partial x^T} \\ \frac{\partial(L_F^0 H)}{\partial x_1}, \frac{\partial(L_F^0 H)}{\partial x_2}, \frac{\partial(L_F^0 H)}{\partial x_3}, \frac{\partial(L_F^0 H)}{\partial x_4} \\ \frac{\partial(L_F^1 H)}{\partial x_1}, \frac{\partial(L_F^1 H)}{\partial x_2}, \frac{\partial(L_F^1 H)}{\partial x_3}, \frac{\partial(L_F^1 H)}{\partial x_4} \\ \frac{\partial(L_F^2 H)}{\partial x_1}, \frac{\partial(L_F^2 H)}{\partial x_2}, \frac{\partial(L_F^2 H)}{\partial x_3}, \frac{\partial(L_F^2 H)}{\partial x_4} \\ \frac{\partial(L_F^3 H)}{\partial x_1}, \frac{\partial(L_F^3 H)}{\partial x_2}, \frac{\partial(L_F^3 H)}{\partial x_3}, \frac{\partial(L_F^3 H)}{\partial x_4} \end{bmatrix}_{8 \times 4} \tag{46}$$

where

$$\frac{\partial(L_F^l H)}{\partial x^T} = \begin{bmatrix} \frac{\partial(L_F^l H_1)}{\partial x_1}, \frac{\partial(L_F^l H_1)}{\partial x_2}, \frac{\partial(L_F^l H_1)}{\partial x_3} \\ \frac{\partial(L_F^l H_1)}{\partial x_4}, \frac{\partial(L_F^l H_2)}{\partial x_1}, \frac{\partial(L_F^l H_2)}{\partial x_2} \\ \frac{\partial(L_F^l H_2)}{\partial x_3}, \frac{\partial(L_F^l H_2)}{\partial x_4} \end{bmatrix}, \tag{47}$$

$l = 0, 1, 2, 3.$

When the vehicle is running, the rank of dV is full. The vehicle state is local observability by differential geometry theory.

The output vector d and its derivative vector \dot{d} for vehicle parameters are defined as follows:

$$N = [d; \dot{d}] = [d_1, d_2; \dot{d}_1, \dot{d}_2]. \tag{48}$$

The observability co-distribution matrix is solved by the Jacobian matrix:

$$\nabla N = [\partial N / \partial M_t, \partial N / \partial L_f, \partial N / \partial I_z]_{4 \times 3}. \tag{49}$$

Some derivatives can be solved as follows:

$$\left\{ \begin{aligned} \frac{\partial d_1}{\partial M_t} &= 0, \frac{\partial d_2}{\partial I_z} = 0, \\ \frac{\partial d_2}{\partial M_t} &= -\frac{1}{M_t^2} \left(F_{ty}^{fl} \cos \tau_{fl} + F_{tx}^{fl} \sin \tau_{fl} + F_{ty}^{fr} \cos \tau_{fr} + F_{tx}^{fr} \sin \tau_{fr} + F_{ty}^{rr} + F_{tx}^{rr} \right), \\ \frac{\partial \dot{d}_1}{\partial L_f} &= \frac{1}{I_z} \left(F_{tx}^{fl} \sin \tau_{fl} + F_{ty}^{fl} \cos \tau_{fl} + F_{tx}^{fr} \sin \tau_{fr} + F_{ty}^{fr} \cos \tau_{fr} \right), \\ \frac{\partial \dot{d}_1}{\partial I_z} &= -\frac{1}{I_z^2} \left((F_{ty}^{fl} \sin \tau_{fl} - F_{tx}^{fl} \cos \tau_{fl}) B_l + (F_{tx}^{fr} \cos \tau_{fr} - F_{ty}^{fr} \sin \tau_{fr}) B_r - (F_{ty}^{rr} + F_{tx}^{rr}) L_r + (F_{tx}^{fl} \sin \tau_{fl} + F_{ty}^{fl} \cos \tau_{fl} + F_{tx}^{fr} \sin \tau_{fr} + F_{ty}^{fr} \cos \tau_{fr}) L_f + (F_{tx}^{rr} B_r - F_{tx}^{rl} B_l) \right). \end{aligned} \right. \tag{50}$$

It can be easily obtained from the above partial derivative equation that ∇N is full rank when the vehicle is in the steering mode. Thus the vehicle parameter vector $\theta(t)$ has local observability.

The state equation and measurement equation of vehicle system discretized by sampling time are:

$$x(t) = \begin{bmatrix} \beta(t) \\ r_z(t) \\ v_x(t) \\ a_y(t) \end{bmatrix} = \begin{bmatrix} \left(a_y(t-1) - \beta(t-1) a_x(t-1) \right) \\ -v_x(t-1) r_z(t-1) \\ -\beta(t-1)^2 v_x(t-1) r_z(t-1) \\ r_z(t-1) + T_s M_z(t-1) / I_z(t-1) \\ v_x(t-1) + T_s \left(a_x + v_x(t-1) \right) \\ \sum F_{ty}^{ij}(t-1) / M_t(t-1) \end{bmatrix}, \tag{51}$$

$$\begin{aligned} \sum F_{ty}^{ij}(t-1) &= F_{ty}^{fl}(t-1) \cos \tau_{fl}(t-1) + F_{ty}^{rr}(t-1) \\ &+ F_{ty}^{rl}(t-1) + F_{tx}^{fl}(t-1) \sin \tau_{fl}(t-1) \\ &+ F_{ty}^{fr}(t-1) \cos \tau_{fr}(t-1) \\ &+ F_{tx}^{rl}(t-1) \sin \tau_{fr}(t-1), \end{aligned} \tag{52}$$

$$\begin{aligned} M_z(t-1) &= B_l \left(F_{ty}^{fl}(t-1) \sin \tau_{fl}(t-1) - F_{tx}^{fl}(t-1) \cos \tau_{fl}(t-1) \right) - L_r \left(F_{ty}^{rr}(t-1) + F_{tx}^{rl}(t-1) \right) \\ &+ \left(F_{tx}^{rr}(t-1) B_r - F_{tx}^{rl}(t-1) B_l \right) + \left(F_{ty}^{fl}(t-1) \cos \tau_{fl}(t-1) + F_{tx}^{fl}(t-1) \sin \tau_{fl}(t-1) \right) \\ &L_f(t-1) - L_r \left(F_{ty}^{fr}(t-1) \sin \tau_{fr}(t-1) - F_{tx}^{fr}(t-1) \cos \tau_{fr}(t-1) \right) + \left(F_{ty}^{fr}(t-1) \cos \tau_{fr}(t-1) + F_{tx}^{fr}(t-1) \sin \tau_{fr}(t-1) \right) \\ &L_f(t-1). \end{aligned} \tag{53}$$

The discrete equation of vehicle parameters to be estimated is as follows:

$$\theta(t) = \begin{bmatrix} M_t(t-1) \\ L_f(t-1) \\ L_z(t-1) \end{bmatrix}. \quad (54)$$

The observation process of state and parameters of the DCDKF is divided into four parts: Parameter prediction, state prediction, parameter correction and state correction [24, 32]. The specific process is derived as follows.

Step 1: Initialize system variables

Here, the values that need initialization include

$$\hat{\mathbf{x}}(0), \mathbf{P}_x(0), \hat{\theta}(0), \mathbf{P}_\theta(0), \mathbf{Q}_x, \mathbf{R}_x, \mathbf{Q}_\theta, \mathbf{R}_\theta.$$

Step 2: Time update of time-varying parameters

$$\begin{cases} \hat{\theta}(t|t-1) = \hat{\theta}(t-1|t-1), \\ \hat{\mathbf{P}}_\theta(t|t-1) = \hat{\mathbf{P}}_\theta(t-1|t-1) + \mathbf{Q}_\theta. \end{cases} \quad (55)$$

Step 3: Time update of vehicle state to be estimated

The sigma point set for vehicle state variables is created as:

$$\mathbf{X}_i(t-1|t-1) = \begin{bmatrix} \hat{\mathbf{x}}(t-1|t-1) - h\sqrt{\hat{\mathbf{P}}_x(t-1|t-1)} \\ \hat{\mathbf{x}}(t-1|t-1) \\ \hat{\mathbf{x}}(t-1|t-1) + h\sqrt{\hat{\mathbf{P}}_x(t-1|t-1)} \end{bmatrix}, \quad (56)$$

$$\begin{cases} \mathbf{X}_i(t-1|t-1) = \hat{\mathbf{x}}(t-1|t-1), & i = 0, \\ \mathbf{X}_i(t-1|t-1) = \hat{\mathbf{x}}(t-1|t-1) + \left(h\sqrt{\hat{\mathbf{P}}_x(t-1|t-1)}\right)_i, & i = 1, 2, \dots, N_x, \\ \mathbf{X}_i(t-1|t-1) = \hat{\mathbf{x}}(t-1|t-1) - \left(h\sqrt{\hat{\mathbf{P}}_x(t-1|t-1)}\right)_i, & i = N_x + 1, \dots, 2N_x, \end{cases} \quad (57)$$

and the corresponding weight is:

$$\begin{cases} \tau_{x,0}^m = \tau_{x,0}^c = \frac{h^2 - N_x}{h^2}, & i = 0, \\ \tau_{x,i}^m = \tau_{x,i}^c = \frac{1}{2h^2}, & i = 1, 2, \dots, 2N_x. \end{cases} \quad (58)$$

The set of conductive sigma point of state is:

$$\mathbf{X}_i(t|t-1) = \mathbf{f}\left(\mathbf{X}_i(t-1|t-1), \hat{\theta}(t|t-1), \mathbf{u}(t-1)\right). \quad (59)$$

The predictive value of the vehicle state is calculated as:

$$\hat{\mathbf{x}}(t|t-1) = \sum_{i=0}^{2N_x} \tau_{x,i}^m \mathbf{X}_i(t|t-1), \quad (60)$$

and its covariance matrix is:

$$\begin{aligned} \hat{\mathbf{P}}_x(t|t-1) &= \sum_{i=0}^{2N_x} \tau_{x,i}^c \left(\mathbf{X}_i(t|t-1) - \hat{\mathbf{x}}(t|t-1)\right) \\ &\quad \left(\mathbf{X}_i(t|t-1) - \hat{\mathbf{x}}(t|t-1)\right)^T + \mathbf{Q}_x, \end{aligned} \quad (61)$$

where N_x is the vehicle state dimension to be estimated, and $N_x=4$.

Step 4: Calculate the sigma point set for parameters

$$\varsigma_j(t|t-1) = \begin{bmatrix} \hat{\theta}(t|t-1) - h\sqrt{\hat{\mathbf{P}}_\theta(t|t-1)} \hat{\theta}(t|t-1) \\ \hat{\theta}(t|t-1) + h\sqrt{\hat{\mathbf{P}}_\theta(t|t-1)} \end{bmatrix}, \quad (62)$$

$$\begin{cases} \varsigma_j(t|t-1) = \hat{\theta}(t|t-1), & j = 0, \\ \varsigma_j(t|t-1) = \hat{\theta}(t|t-1) + \left(h\sqrt{\hat{\mathbf{P}}_\theta(t|t-1)}\right)_j, & j = 1, 2, \dots, N_\theta, \\ \varsigma_j(t|t-1) = \hat{\theta}(t|t-1) - \left(h\sqrt{\hat{\mathbf{P}}_\theta(t|t-1)}\right)_j, & j = N_\theta + 1, \dots, 2N_\theta, \end{cases} \quad (63)$$

where N_θ is the vehicle parameter dimension to be estimated, and $N_\theta=3$. And the corresponding weight is:

$$\begin{cases} \tau_{\theta,0}^m = \tau_{\theta,0}^c = \frac{h^2 - N_\theta}{h^2}, & j = 0, \\ \tau_{\theta,j}^m = \tau_{\theta,j}^c = \frac{1}{2h^2}, & j = 1, 2, \dots, 2N_\theta. \end{cases} \quad (64)$$

h is the half step of central difference, and $h=\sqrt{3}$.

Step 5: Measurement update output for the vehicle parameter

$$\begin{cases} \mathbf{y}_\theta^j(t|t-1) = \mathbf{h}\left(\mathbf{f}\left(\hat{\mathbf{x}}(t-1|t-1), \mathbf{u}(t-1), \right.\right. \\ \left.\left. \varsigma_j(t|t-1)\right), \mathbf{u}(t), \varsigma_j(t|t-1)\right), \\ \hat{\mathbf{y}}_\theta(t|t-1) = \sum_{i=0}^{2N_\theta} \tau_{\theta,i}^m \mathbf{y}_\theta^i(t|t-1). \end{cases} \quad (65)$$

Step 6: Measurement output update for the vehicle state

$$\begin{cases} \mathbf{y}_x^i(t|t-1) = \mathbf{h}\left(\mathbf{X}_i(t|t-1), \mathbf{u}(k), \hat{\theta}(t|t-1)\right), \\ \hat{\mathbf{y}}_x(t|t-1) = \sum_{i=0}^{2N_x} \tau_{x,i}^m \mathbf{y}_x^i(t|t-1). \end{cases} \quad (66)$$

Step 7: Update covariance for the vehicle state

The innovation covariance for the vehicle state can be given as:

$$\begin{aligned} \hat{\mathbf{P}}_{\hat{\mathbf{y}}_x \hat{\mathbf{y}}_x}(t|t-1) &= \sum_{i=0}^{2N_x} \tau_{x,i}^c \left(\mathbf{y}_x^i(t|t-1) - \hat{\mathbf{y}}_x(t|t-1)\right) \\ &\quad \times \left(\mathbf{y}_x^i(t|t-1) - \hat{\mathbf{y}}_x(t|t-1)\right)^T + \mathbf{R}_s. \end{aligned} \quad (67)$$

The cross-covariance matrix for the vehicle state is presented as:

$$\hat{\mathbf{P}}_{\hat{\mathbf{x}}\hat{\mathbf{y}}_x}(t|t-1) = \sum_{i=0}^{2N_x} \tau_{x,i}^c (\mathbf{X}_i(t|t-1) - \hat{\mathbf{x}}(t|t-1)) (\mathbf{y}_x^i(t|t-1) - \hat{\mathbf{y}}_x(t|t-1))^T. \quad (68)$$

And the gain of filter of the vehicle for state estimation can be presented as:

$$\mathbf{G}_x = \hat{\mathbf{P}}_{\hat{\mathbf{x}}\hat{\mathbf{y}}_x}(t|t-1) \hat{\mathbf{P}}_{\hat{\mathbf{y}}_x\hat{\mathbf{y}}_x}^{-1}(t|t-1). \quad (69)$$

Step 8: Update covariance for parameter

The innovation covariance for the vehicle parameter can be calculated as:

$$\hat{\mathbf{P}}_{\hat{\mathbf{y}}_\theta\hat{\mathbf{y}}_\theta}(t|t-1) = \sum_{j=0}^{2N_\theta} \tau_{\theta,j}^c (\mathbf{y}_\theta^j(t|t-1) - \hat{\mathbf{y}}_\theta(t|t-1)) (\mathbf{y}_\theta^j(t|t-1) - \hat{\mathbf{y}}_\theta(t|t-1))^T + \mathbf{R}_\theta. \quad (70)$$

The cross-covariance matrix for the vehicle parameter is as follows:

$$\hat{\mathbf{P}}_{\hat{\mathbf{y}}_\theta\hat{\mathbf{y}}_x}(t|t-1) = \sum_{j=0}^{2N_\theta} \tau_{\theta,j}^c (\mathbf{s}_j(t|t-1) - \hat{\boldsymbol{\theta}}(t|t-1)) (\mathbf{y}_\theta^j(t|t-1) - \hat{\mathbf{y}}_\theta(t|t-1))^T. \quad (71)$$

And the gain of filter of the vehicle for parameter estimation can be obtained as:

$$\mathbf{G}_\theta = \hat{\mathbf{P}}_{\hat{\mathbf{y}}_\theta\hat{\mathbf{y}}_x}(t|t-1) \hat{\mathbf{P}}_{\hat{\mathbf{y}}_\theta\hat{\mathbf{y}}_\theta}^{-1}(t|t-1). \quad (72)$$

Step 9: Correct state

The optimal value of current state can be calculated as:

$$\hat{\mathbf{x}}(t|t) = \hat{\mathbf{x}}(t|t-1) + \mathbf{G}_x (\mathbf{y}_x - \hat{\mathbf{y}}_x(t|t-1)). \quad (73)$$

The covariance matrix for state estimation can be updated as follows:

$$\hat{\mathbf{P}}_x(t|t) = \hat{\mathbf{P}}_x(t|t-1) - \mathbf{G}_x \hat{\mathbf{P}}_{\hat{\mathbf{y}}_x\hat{\mathbf{y}}_x}(t|t-1) \mathbf{G}_x^T. \quad (74)$$

Step 10: Correct parameter

The optimal value of current parameter can be calculated as:

$$\hat{\boldsymbol{\theta}}(t|t) = \hat{\boldsymbol{\theta}}(t|t-1) + \mathbf{G}_\theta (\mathbf{y}_\theta - \hat{\mathbf{y}}_\theta(t|t-1)). \quad (75)$$

The covariance matrix for parameter estimation can be updated as follows:

$$\hat{\mathbf{P}}_\theta(t|t) = \hat{\mathbf{P}}_\theta(t|t-1) - \mathbf{G}_\theta \hat{\mathbf{P}}_{\hat{\mathbf{y}}_\theta\hat{\mathbf{y}}_\theta}(t|t-1) \mathbf{G}_\theta^T. \quad (76)$$

Remark 1: Note that the designed DCDKF approach is feasible and available in this study, because the DCDKF utilizes ‘boot-strapping’ technique to synchronously estimate vehicle inertial parameters and system states, two KFs operate in parallel, and the two KFs exchange information with each other and use each other’s estimators as prior information for the next step, so as to the DCDKF can improve the estimation accuracy of vehicle inertial parameters and system states. Similar dual Kalman filter estimation strategies have been validated for other states and parameters [24, 25, 27, 28].

Remark 2: It is fact that the vehicle estimation system also exists other challenges such as external interference, strong nonlinearity, undesirable signal bias and noise oscillation, and other complex conditions, which requires to develop and design adaptive estimators or nonlinear observers to improve the estimation accuracy of the estimator in the future. Different from the proposed estimation method, the observability proof of the nonlinear observer will use the Lyapunov stability rather than observability co-distribution matrix of full rank. Besides, since the CDKF is developed from the classical Kalman filter that can performs optimal estimation of system state in the presence of noise and interference, which has been proved to possess ability in dealing with the estimation and observation errors [24, 32], here theoretical foundations for estimation errors of such observer are omitted, interested readers can refer to other Refs. [16, 21, 24, 32].

4 Simulation and Analysis

To verify the estimation performance of the DCDKF on vehicle state and parameters, different driving maneuvers are implemented in the high-fidelity co-simulation platform of MATLAB/Simulink-Carsim[®] environment, which is established based on the principle of joint estimation shown in Figure 4. And the co-simulation communication between CarSim and MATLAB/Simulink is realized through the connection interface of Carsim[®]-S function. Note that this model in Carsim[®] is mainly aimed at conventional vehicles rather than electric vehicles, thus the co-simulation platform consists of the vehicle dynamics and tire model in Carsim[®] and electric drive system model in MATLAB/Simulink. In the simulation, the main parameters of the whole vehicle are shown in Table 2. The driving road condition of the vehicle is set as the asphalt pavement with high friction coefficient. The simulation time is 20 s and the sampling time is 0.001 s.

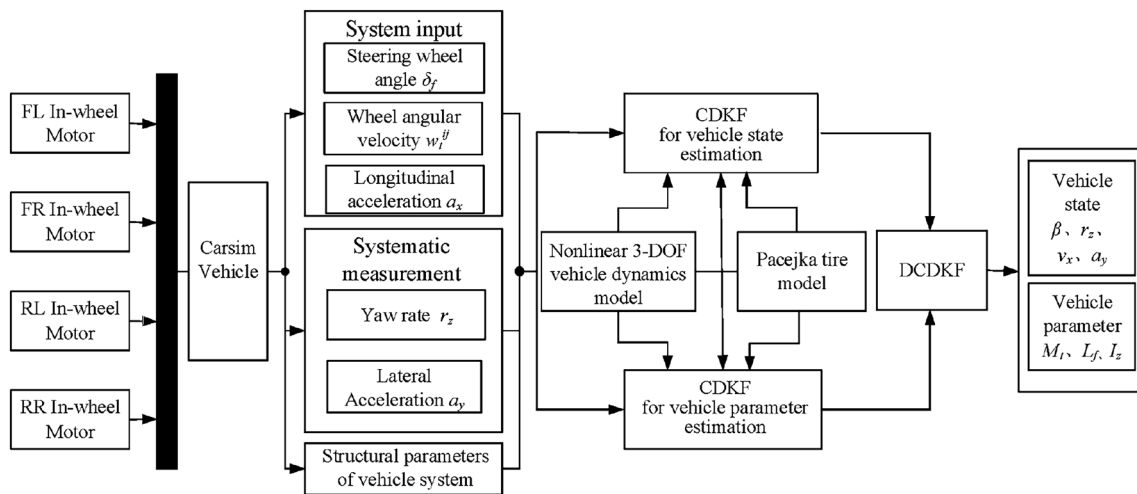


Figure 4 Framework of simulation platform for the joint estimation of state and parameters

Table 2 Main parameters of the whole vehicle

Parameter	Value	Parameter	Value
M_t (kg)	1171	H (m)	0.3
C_a	0.33	I_z (kg·m ²)	2031
P_a (kg/m ³)	1.206	R_e (m)	0.3
S (m ²)	1.6	I_{wt} (kg·m)	2.1
L_f (m)	1.04	C_e (V/(r/min))	0.01675
L_r (m)	1.56	C_m (N·m/A)	0.16
B_l (m)	0.7405	L_m (H)	1.5×10^{-3}

4.1 Comparison Between DCDKF and DEKF

In order to evaluate the observation effect of DCDKF observer on the vehicle state and parameters, the steering wheel angle for the snake-like steering (SLS) manoeuvre as shown in Figure 5 is adopted, and the estimation result is compared with that of dual extended Kalman filter (DEKF) observer. The results of state and parameters jointly estimated by DEKF and DCDKF are shown in Figures 6, 7, 8, 9, 10, 11, respectively. Among the results, the estimated vehicle state consisting of the sideslip angle at CG, yaw rate and longitudinal velocity are shown in Figures 6, 7, 8, whereas the estimated vehicle parameters including the mass of the whole vehicle, the horizontal distance from the CG to the front axle and the yaw moment of inertia are shown in Figures 9, 10, 11.

From the comparison chart of simulation results, it can be concluded that except for the relatively obvious error of sideslip angle at CG, the other estimated results converge to the true value with little deviation, and the error

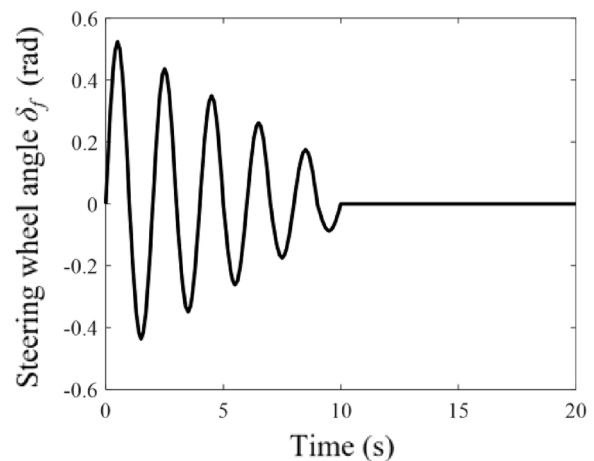


Figure 5 Steering wheel angle for SLS

of sideslip angle at CG may be caused by the unmodeled dynamic characteristics of vehicle system, or the influence of inaccurate modeling parameters on filtering accuracy. It can be seen from the local enlarged figure of the results that the estimation effect of the DCDKF observer is better than that of DEKF observer when estimating the sideslip angle at CG, yaw rate, vehicle mass, horizontal distance from CG to vehicle front axle and yaw moment of inertia. It can be explained as the DCDKF algorithm can avoid the high-order truncation error caused by using Jacobian matrix linearization to approximate nonlinear estimation system through central difference

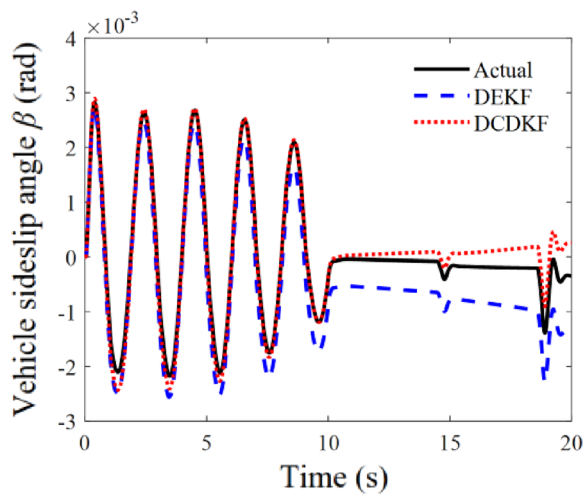


Figure 6 Vehicle sideslip angle for SLS

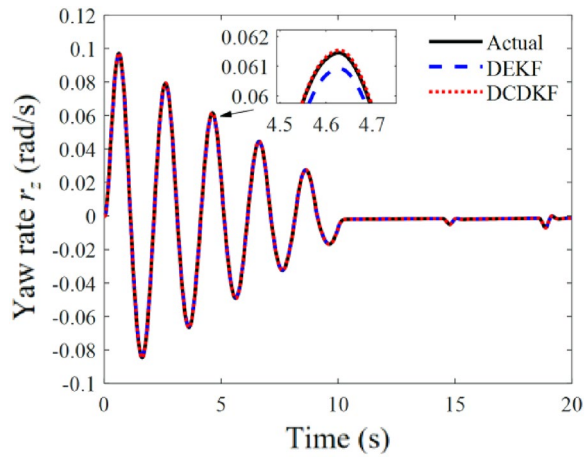


Figure 7 Yaw rate for SLS

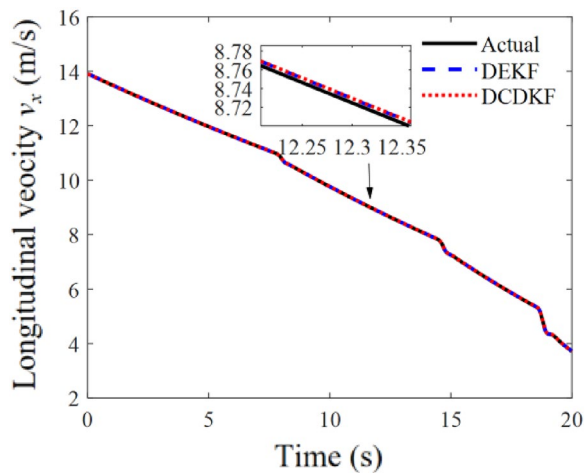


Figure 8 Longitudinal velocity for SLS

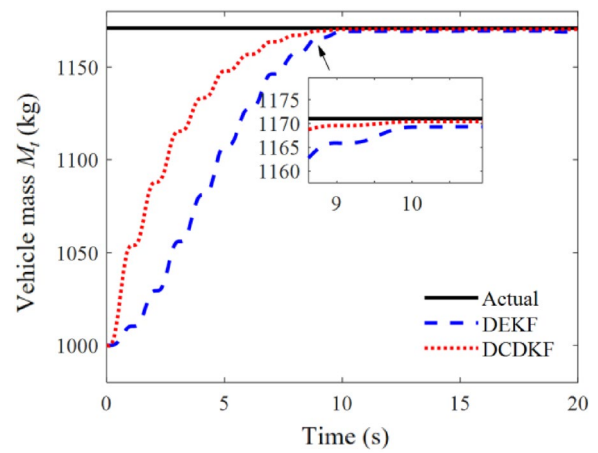


Figure 9 Vehicle mass for SLS

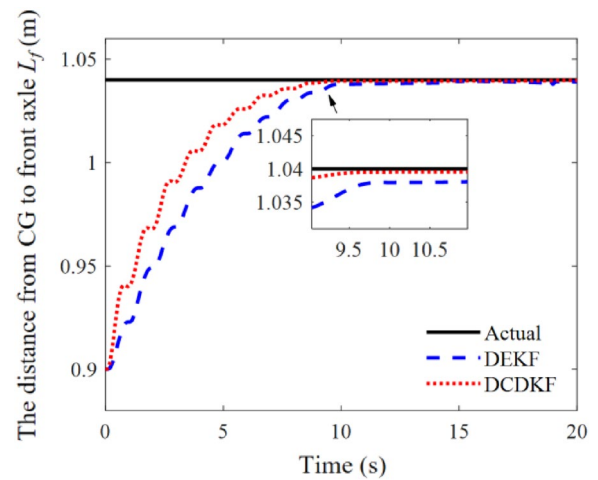


Figure 10 Distance from CG to front axle for SLS

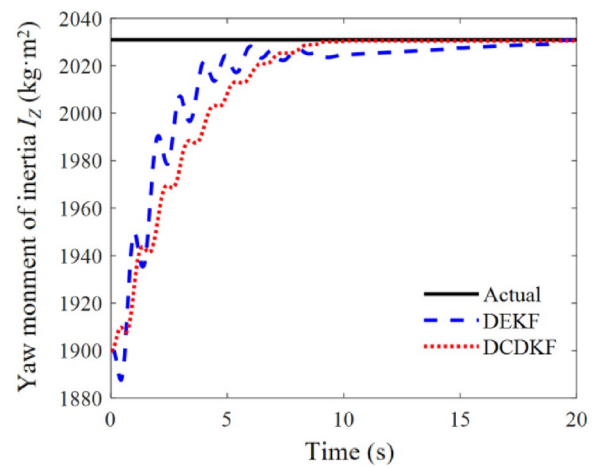


Figure 11 Yaw moment of inertia for SLS

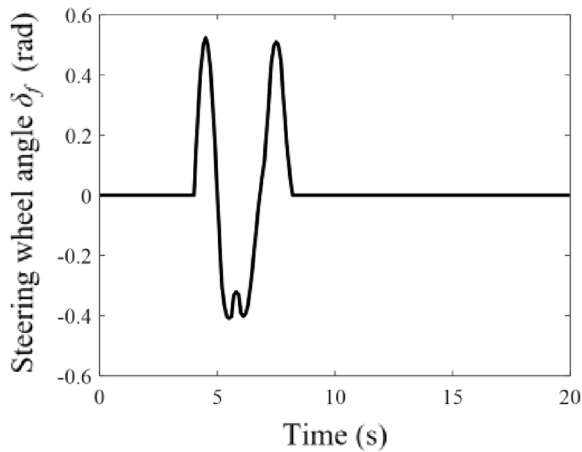


Figure 12 Steering wheel angle for DLC

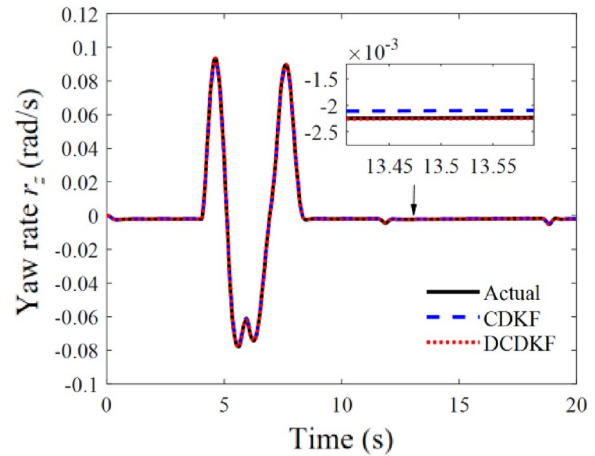


Figure 14 Yaw rate for DLC under $M_p = 80$ kg

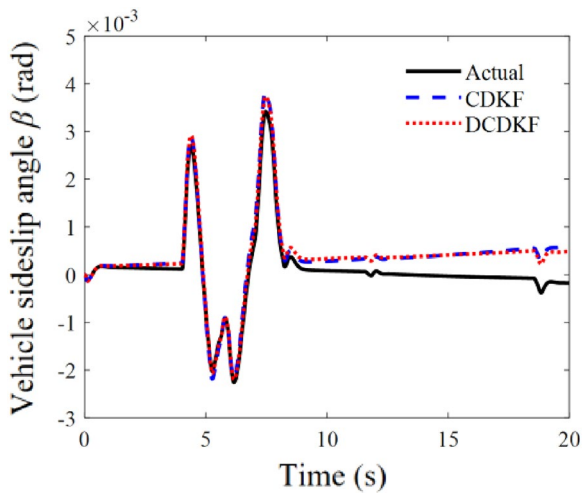


Figure 13 Vehicle sideslip angle for DLC under $M_p = 80$ kg

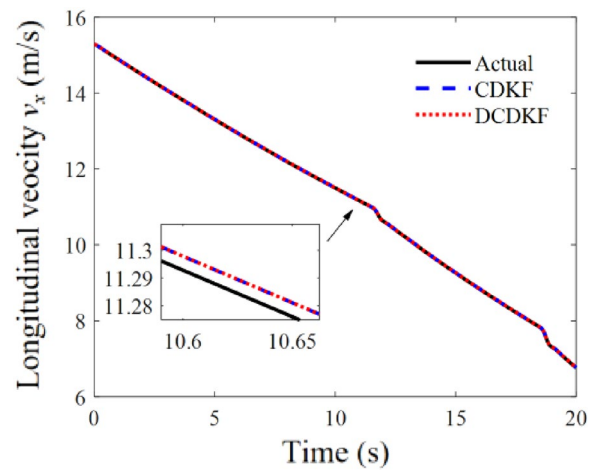


Figure 15 Longitudinal velocity for DLC under $M_p = 80$ kg

transformation, and the DCDKF method has better adaptability to nonlinear vehicle dynamics estimation system.

4.2 Comparison Between CDKF and DCDKF with Different Loads

In order to further analyze the observation effectiveness of the DCDKF algorithm on vehicle state estimation, the simulation is performed under different loads $M_p=80$ kg and $M_p=180$ kg by using double lane change (DLC) manoeuvre, as shown in Figure 12. Figures 13, 14, 15, 16, 17, 18 show the comparison diagram of vehicle state observation results under different loads, respectively. Figures 13, 14, 15 show the results by CDKF and DCDKF algorithm when $M_p=80$ kg, and Figures 16, 17, 18 present the results by CDKF and DCDKF algorithm when $M_p=180$ kg.

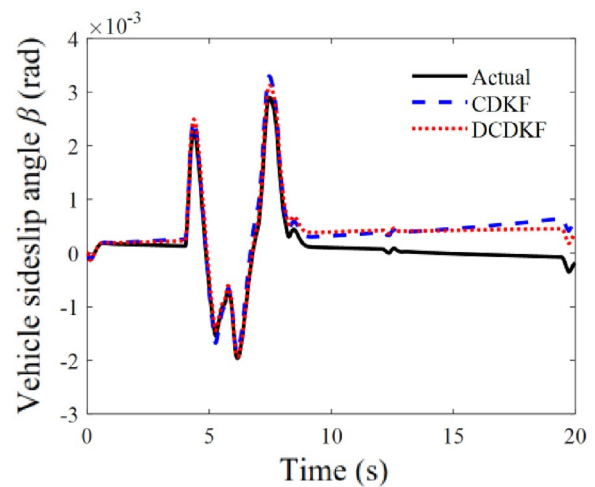


Figure 16 Vehicle sideslip angle for DLC under $M_p = 180$ kg

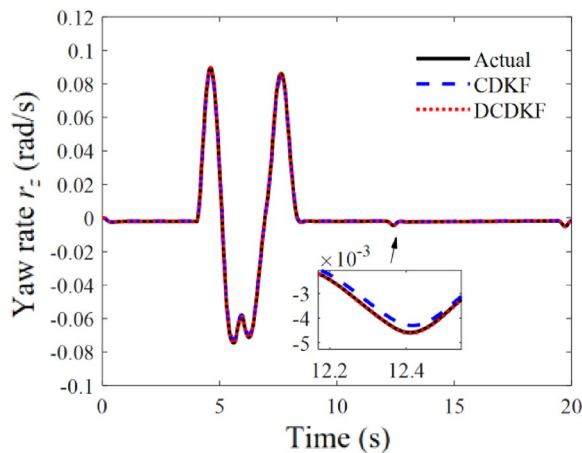


Figure 17 Yaw rate for DLC under $M_p = 180$ kg

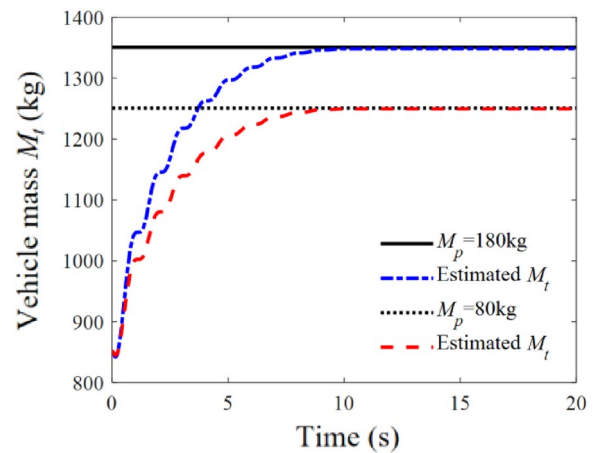


Figure 19 Vehicle mass for SLS of different loads

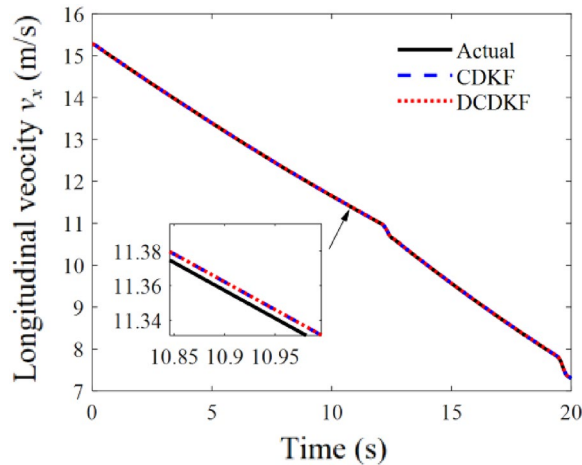


Figure 18 Longitudinal velocity for DLC under $M_p = 180$ kg

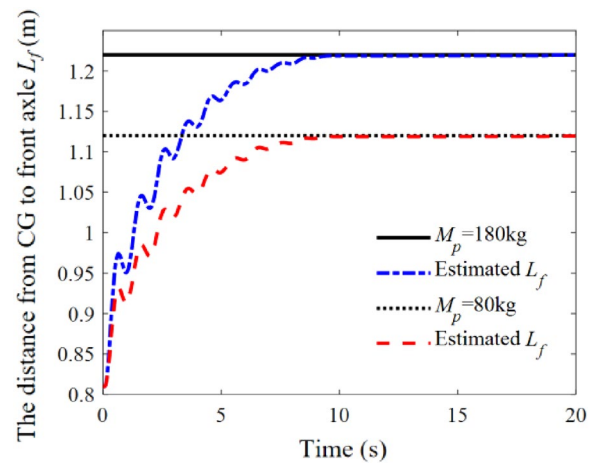


Figure 20 Distance from CG to front axle for SLS of different loads

It can be seen from the results of two sets for the vehicle state estimation that the vehicle state observation effect based on the DCDKF is obviously better than that of single CDKF. This is due to the fact that, compared with using the CDKF to estimate vehicle state alone, the observation system using two parallel CDKF can effectively improve the effect of single estimation and observation accuracy. In other words, DCDKF can use parameters estimation to improve the state observation effect in real time during observation process.

4.3 DCDKF Estimation for Parameters with Different Loads

In order to further verify the effectiveness of the DCDKF for vehicle parameters estimation, different loads of $M_p = 80$ kg and $M_p = 180$ kg are added respectively on the DDEVs. It is worth noting that the load is a point mass,

its own the moment of inertia at the CG is not taken into account. The results of DCDKF observer for vehicle parameters are mainly shown in Figures 19, 20, 21, 22, 23, 24. The observation results of vehicle parameters under different loads under SLS are shown in Figures 19, 20, 21, and the observation results under single sinusoidal steering (SSS) manoeuvre are shown in Figures 22, 23, 24.

As can be seen from these observation results, the DCDKF observer oscillates relatively little in the observation transient process under SLS and SSS with two different loads $M_p = 80$ kg and $M_p = 180$ kg. Meanwhile, in the final steady-state observation results, the steady-state observation values of the DCDKF are basically consistent with the real values. Even when the large load $M_p = 180$ kg is loaded, the DUKF observer still has good observation accuracy.

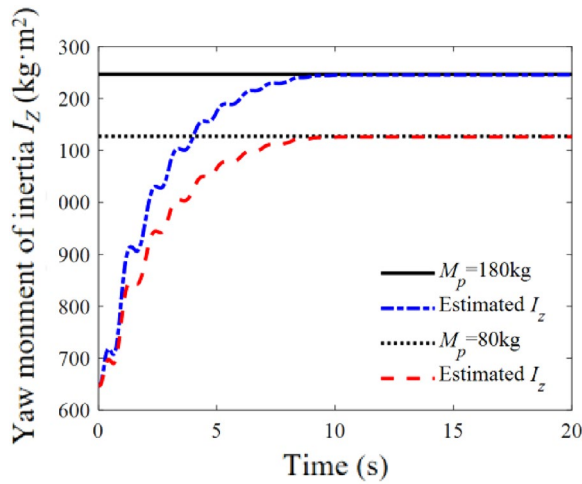


Figure 21 Yaw moment of inertia for SLS of different loads

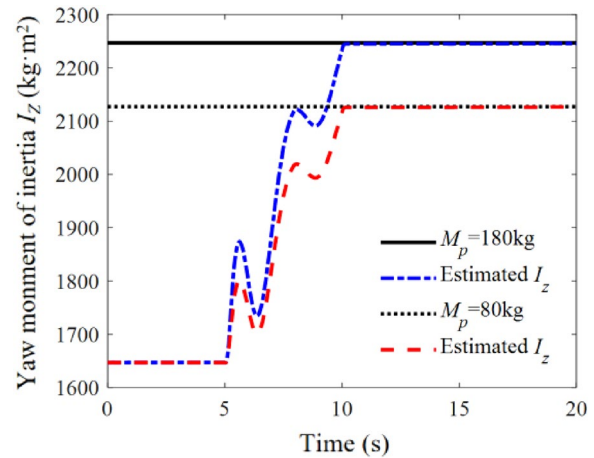


Figure 24 Yaw moment of inertia for SSS of different loads

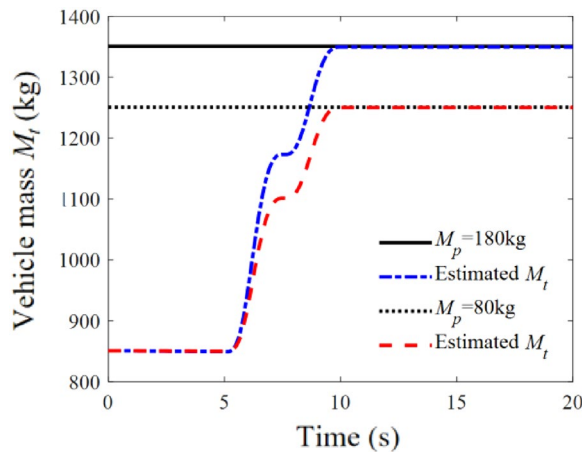


Figure 22 Vehicle mass for SSS of different loads

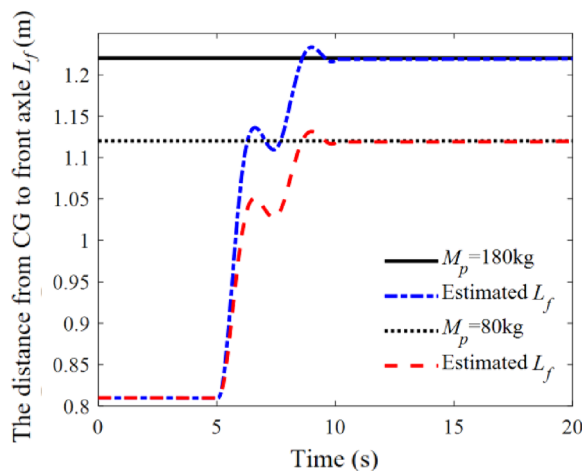


Figure 23 Distance from CG to front axle for SSS of different loads

In summary, the simulation results implemented by different manoeuvre indicate that the proposed DCDKF observer can estimate the vehicle state and parameters with good accuracy under different loads. Furthermore, the proposed DCDKF observer is better able to deal with the non-linear challenge for parameters estimation of strongly nonlinear vehicle system compared with the DEKF observer. Besides, since the CDKF is developed from Kalman filter that has advantages of good stability, real-time fast update and process ability for engineering application, perhaps the computational time of CDKF is slightly higher than Kalman filter, whereas the computational load can be tolerated for vehicle engineering application with advanced on-board processor.

5 Conclusions

- (1) This paper focuses on the estimation of vehicle inertia parameters for DDEVs. Vehicle payload parameter variations including vehicle mass and yaw moment of inertia were analyzed, then the estimation-oriented nonlinear vehicle dynamics model of DDEV considering payload variations was developed.
- (2) The real-time DCDKF estimation of vehicle inertia parameters for DDEVs was proposed and designed with in-vehicle sensors, and local observability of DCDKF was derived via Lie derivative and differential geometry theory. To address system nonlinearities in vehicle dynamics estimation, the DCDKF and DEKF were also investigated and compared. The simulation results with different maneuvers verified effectiveness of the proposed DCDKF with different payloads.

- (3) Furthermore, this paper revealed that potential effects of variations of inertial parameters for vehicle dynamics control system should be concerned, and advanced estimation techniques such as adaptive estimators and nonlinear observers should be developed and studied for vehicle dynamic states and parameters in future works.

Acknowledgements

Not applicable.

Authors' Contributions

XJ in charge of the whole trial; GY supervised the whole work of this paper; XJ, JY, LX and CW wrote the manuscript; JY and ZW assisted with sampling and laboratory analyses. All authors read and approved the final manuscript.

Authors' Information

Xianjian Jin born in 1986, is currently an assistant professor at *School of Mechatronic Engineering and Automation, Shanghai University, China*. He received his PhD degree from *Southeast University, China*, in 2017. His research interests include vehicle system dynamics and control, autonomous driving technologies, intelligent and connected vehicles.

Junpeng Yang born in 1992, is currently pursuing the M.S. degree at *School of Mechatronic Engineering and Automation, Shanghai University, China*. He received his B.S. degree from *Henan University of Science and Technology, China*, in 2017. His research interests include vehicle dynamic state estimation and parameter identification for electric vehicles.

Liwei Xu born in 1986, is currently an assistant professor at *School of Mechanical Engineering, Southeast University, China*. He received his PhD degree from *Southeast University, China*, in 2019. His research interests include vehicle system dynamics and control, connected vehicles, and autonomous vehicles.

Chongfeng Wei born in 1986, is currently a senior lecturer at *Mechanical and Construction Engineering, Northumbria University, Newcastle, U.K.*, he received his PhD degree in mechanical engineering from *University of Birmingham, Birmingham, U.K.*, in 2015. His research interests include decision making and control of intelligent vehicles, human-centric autonomous driving, cooperative automation.

Zhaoran Wang born in 1999, is currently pursuing the M.S. degree at *School of Mechatronic Engineering and Automation, Shanghai University, Shanghai, China*. He received his B.S. degree from *Hebei University of Technology, Tianjin, China*, in 2021. His research interests include vehicle dynamic state estimation and parameter identification for electric vehicles.

Guodong Yin born in 1976, is currently a professor at *School of Mechanical Engineering, Southeast University, China*. He received his PhD degree from *Southeast University, China*, in 2007. His research interests include vehicle system dynamics and control, automated driving technologies, intelligent and connected ground vehicles.

Funding

Supported by National Natural Science Foundation of China (Grant Nos. 51905329, 51975118), Foundation of State Key Laboratory of Automotive Simulation and Control of China (Grant No. 20181112).

Declarations

Competing Interests

The authors declare no competing financial interests.

Author Details

¹School of Mechatronic Engineering and Automation, Shanghai University, Shanghai 200072, China. ²State Key Laboratory of Automotive Simulation and Control, Jilin University, Changchun 130025, China. ³School of Mechanical Engineering, Southeast University, Nanjing 211189, China. ⁴Mechanical and Construction Engineering, Northumbria University, Newcastle NE1 8ST, UK.

Received: 26 May 2021 Revised: 5 July 2023 Accepted: 10 July 2023
Published online: 17 August 2023

References

- Y F Wang, H Fujimoto, S Hara. Driving force distribution and control for EV with four in-wheel motors: A case study of acceleration on split-friction surfaces. *IEEE Transactions on Industrial Electronics*, 2016, 64(4): 3380-3388.
- Y H Chen, J K Hedrick, K H Guo. A novel direct yaw moment controller for in-wheel motor electric vehicles. *Vehicle System Dynamics*, 2013, 51(6): 925-942.
- X J Jin, J D Wang, X K He, et al. Improving vibration performance of electric vehicles based on in-wheel motor-active suspension system via robust finite frequency control. *IEEE Transactions on Intelligent Transportation Systems*, 2023, 24(2): 1631-1643.
- A Goodarzi, E Esmailzadeh. Design of a VDC system for all-wheel independent drive vehicles. *IEEE/ASME Transactions on Mechatronics*, 2007, 12(6): 632-639.
- H Zhang, X J Zhang, J M Wang. Robust gain-scheduling energy-to-peak control of vehicle lateral dynamics stabilisation. *Vehicle System Dynamics*, 2014, 52(3): 309-340.
- X J Jin, Q K Wang, Z Y Yan, et al. A learning-based evaluation for lane departure warning system considering driving characteristics. *Proceedings of the Institution of Mechanical Engineers, Part D: Journal of Automobile Engineering*, 2022.
- X J Jin, J D Wang, Z Y Yan, et al. Robust vibration control for active suspension system of in-wheel-motor-driven electric vehicle via μ -synthesis methodology. *ASME Transactions Journal of Dynamic Systems, Measurement, and Control*, 2022, 144(5): 051007.
- A Farazandeh, A K W Ahmed, S Rakheja. An independently controllable active steering system for maximizing the handling performance limits of road vehicles. *Proceedings of the Institution of Mechanical Engineers, Part D: Journal of Automobile Engineering*, 2015, 229(10): 1291-1309.
- C Hu, Z F Wang, H Taghavifar, et al. MME-EKF-based path-tracking control of autonomous vehicles considering input saturation. *IEEE Transactions on Vehicular Technology*, 2019, 68(6): 5246-5259.
- S L Perić, D S Antić, M B Milovanović, et al. Quasi-sliding mode control with orthogonal endocrine neural network-based estimator applied in anti-lock braking system. *IEEE/ASME Transactions on Mechatronics*, 2015, 21(2): 754-764.
- W Zhang, X X Guo. An ABS control strategy for commercial vehicle. *IEEE/ASME Transactions on Mechatronics*, 2015, 20(1): 384-392.
- H Y Li, H H Liu, H J Gao, et al. Reliable fuzzy control for active suspension systems with actuator delay and fault. *IEEE Transactions on Fuzzy Systems*, 2011, 20(2): 342-357.
- D Saifia, M Chadli, H R Karimi, et al. Fuzzy control for electric power steering system with assist motor current input constraints. *Journal of the Franklin Institute*, 2015, 352(2): 562-576.
- G Reina, M Paiano, J L Blanco-Claraco. Vehicle parameter estimation using a model-based estimator. *Mechanical Systems and Signal Processing*, 2017, 87: 227-241.
- Y Sun, L Li, B J Yan, et al. A hybrid algorithm combining EKF and RLS in synchronous estimation of road grade and vehicle' mass for a hybrid electric bus. *Mechanical Systems and Signal Processing*, 2016, 68: 416-430.
- J Chen, J Song, L Li, et al. UKF-based adaptive variable structure observer for vehicle sideslip with dynamic correction. *IET Control Theory & Applications*, 2016, 10(14): 1641-1652.
- M Gadola, D Chindamo, M Romano, et al. Development and validation of a Kalman filter-based model for vehicle slip angle estimation. *Vehicle System Dynamics*, 2014, 52(1): 68-84.
- K Nam, S Oh, H Fujimoto, et al. Estimation of sideslip and roll angles of electric vehicles using lateral tire force sensors through RLS and Kalman filter approaches. *IEEE Transactions on Industrial Electronics*, 2012, 60(3): 988-1000.
- F Di Biase, B Lenzo, F Timpone. Vehicle sideslip angle estimation for a heavy-duty vehicle via extended Kalman filter using a rational tyre model. *IEEE Access*, 2020, 8: 142120-142130.

- [20] Z Q Qi, S Taheri, B F Wang, et al. Estimation of the tyre–road maximum friction coefficient and slip slope based on a novel tyre model. *Vehicle System Dynamics*, 2015, 53(4): 506-525.
- [21] J Stéphant, A Charara, D Meizel. Virtual sensor: Application to vehicle side-slip angle and transversal forces. *IEEE Transactions on Industrial Electronics*, 2004, 51(2): 278-289.
- [22] Y H Chen, Y F Ji, K H Guo. A reduced-order nonlinear sliding mode observer for vehicle slip angle and tyre forces. *Vehicle System Dynamics*, 2014, 52(12): 1716-1728.
- [23] X Y Zhu, W Li. Takagi–Sugeno fuzzy model based shaft torque estimation for integrated motor–transmission system. *ISA Transactions*, 2019, 93: 14-22.
- [24] X J Jin, G D Yin, N Chen. Advanced estimation techniques for vehicle system dynamic state: A survey. *Sensors*, 2019, 19(19): 4289.
- [25] S Lee, K Nakano, M Otori. On-board identification of tyre cornering stiffness using dual Kalman filter and GPS. *Vehicle System Dynamics*, 2015, 53(4): 437-448.
- [26] X Y Huang, J M Wang. Real-time estimation of center of gravity position for lightweight vehicles using combined AKF–EKF method. *IEEE Transactions on Vehicular Technology*, 2014, 63(9): 4221-4231.
- [27] C Lin, X L Gong, R Xiong, et al. A novel H_∞ and EKF joint estimation method for determining the center of gravity position of electric vehicles. *Applied Energy*, 2017, 194: 609-616.
- [28] C Z Cheng, D Cebon. Parameter and state estimation for articulated heavy vehicles. *Vehicle System Dynamics*, 2011, 49(1-2): 399-418.
- [29] W K Wan, J G Feng, B Song, et al. Huber-based robust unscented Kalman filter distributed drive electric vehicle state observation. *Energies*, 2021, 14(3): 750.
- [30] X F Pei, Z F Chen, B Yang, et al. Estimation of states and parameters of multi-axle distributed electric vehicle based on dual unscented Kalman filter. *Science Progress*, 2020, 103(1): 1-20.
- [31] J Lian, S Liu, L H Li, et al. A mixed logical dynamical-model predictive control (MLD-MPC) energy management control strategy for plug-in hybrid electric vehicles (PHEVs). *Energies*, 2017, 10(1): 74.
- [32] H A Tehrani, A Bakhshi, T T Y Yang. Online jointly estimation of hysteretic structures using the combination of central difference Kalman filter and Robbins–Monro technique. *Journal of Vibration and Control*, 2020, 27(1-2): 234-247.
- [33] A Martinelli. Nonlinear unknown input observability: Extension of the observability rank condition. *IEEE Transactions on Automatic Control*, 2018, 64(1): 222-237.
- [34] H Nijmeijer, A J Van der Schaft. *Nonlinear dynamical control systems*. New York: Springer-verlag, 1990.

Submit your manuscript to a SpringerOpen[®] journal and benefit from:

- Convenient online submission
- Rigorous peer review
- Open access: articles freely available online
- High visibility within the field
- Retaining the copyright to your article

Submit your next manuscript at ► [springeropen.com](https://www.springeropen.com)
